ISBN: 978-3-95450-241-7 ISSN: 2673-5350 doi:10.18429/JACoW-IBIC2022-WEP16

PSF CHARACTERIZATION OF THE ALBA X-RAY PINHOLES

U. Iriso, Z. Martí, A. A. Nosych, ALBA Synchrotron, Cerdanyola del Vallès, Spain
A. Cazorla, ICMAB, Campus UAB, Bellaterra, Spain
I. Mases, CERN, Geneva, Switzerland

Abstract

ALBA is currently equipped with two X-ray pinhole cameras for continuous beam size monitoring using the synchrotron radiation from two different bending magnets. The first pinhole was installed on day-1 and it is working properly since 2011 as the work-horse for the ALBA emittance measurements. The second one has been commissioned in early 2021 for redundancy purposes. This paper summarizes the exercises to characterize the Point Spread Function (PSF) of both pinhole cameras using analytical calculations, SRW simulations, and experimental measurements.

INTRODUCTION

Measuring the transverse beam size and emittance of the electron beam is an essential tool to control the machine performance. Since the ALBA commissioning in 2011, this was carried out using an X-ray pinhole camera located in FE34 [1]. During the last years, at ALBA we have performed other means to infer the beam emittance based on the Synchrotron Radiation Interferometry (SRI) [2] or Heterodyne Near Field Speckles (HNFS) [3]. Nevertheless, we found the X-ray pinhole camera as a more robust set-up, and so we have finally decided to install a second unit for redundancy purposes, this time located in FE21 - almost on the opposite side of the storage ring.

In a pinhole (see Fig. 1), the source image (the electron beam) is amplified at the image plane by a factor $X = L_2/L_1$, where L_1 is the distance between the source point and the pinhole, and L_2 corresponds to the distance between the pinhole and the image plane (YAG screen).

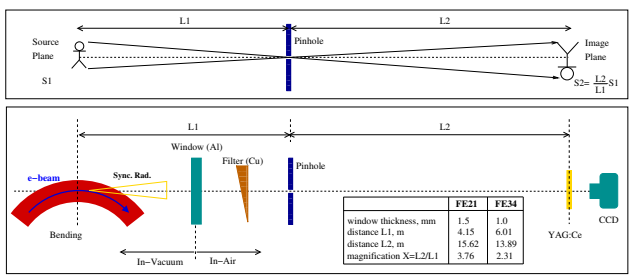

Figure 1: Top: general working principle of a pinhole imaging system. Bottom: sketch of the X-ray pinhole cameras at ALBA, with the geometrical parameters of FE21 and FE34.

But imaging with a pinhole requires a thorough characterization of the pinhole Point Spread Function (PSF, or σ_{PSF} in the following), which is the beam size measured at the image plane corresponding to a point-like source. If σ_e is the electron beam size, the size measured at the YAG screen in Fig. 1 is affected by the σ_{PSF} by:

$$\sigma^2_{\mathrm{YAG}} = (X\sigma_e)^2 + \sigma^2_{\mathrm{PSF}} \,. \quad (1)$$

This paper summarizes the exercises to characterize the PSF of both ALBA pinhole cameras using analytical calculations, SRW simulations [4], and experimental measurements using the beam lifetime. For reference, Table 1 lists the main beam parameters for both pinholes.

Table 1: Twiss Parameters at FE21 and FE34, and Main Operation Parameters of ALBA

	FE21	FE34
hor beam size, µm	55	60
ver beam size, µm	24	27
hor beta function, m	0.52	0.435
ver beta function, m	22.83	25.82
hor dispersion, mm	20.1	37.1
ver dispersion, mm	7.0	11.5
energy spread, %	$1.05{\cdot}10^{-3}$	
emittance, nm·rad	4.6	
coupling, %	0.5	
energy, GeV	2.98	

BEAMLINE SETUP

Both ALBA set-ups (see Fig. 1, bottom) follow the classical design in other light sources [5]: the source point (a bending dipole in both cases) emits synchrotron radiation, and the visible and soft X-rays part are filtered out by an Aluminium window. Furthermore, the Al-window separates vacuum from in-air components. Next a Copper filter whose length can be varied between 0 mm and 5 mm is used to attenuate or harden the X-rays before they hit the pinhole. This is a µm size hole, which is properly aligned using a motorized stage (see next sub-section). Finally, an imaging system consisting in a YAG screen with an optical set-up transforms the X-rays into visible light to form the image and obtain the beam size.

The paper focuses on the cases with and without the use of Cu filter. By optimizing the contrast in Control Room during normal operation conditions, we work with a Cu thickness of 0.3 mm. In order to compare the Cu filter effect, the paper focus the study on four cases:

(a) FE21, 1.5 mm of Al

(b) FE21, 1.5 mm of Al, and 0.3 mm of Cu

(c) FE34, 1.0 mm of Al

(d) FE34, 1.0 mm of Al, and 0.3 mm of Cu

ISBN: 978-3-95450-241-7 ISSN: 2673-5350 doi:10.18429/JACoW-IBIC2022-WEP16

As an illustrative example, Fig. 2 shows the spectrum of the FE34 coming from an ALBA dipole, and after traversing the 1 mm of Al (case "c"), and [1 mm of Al plus 0.3 mm of Cu] (case "d"). Note that with only 0.3 mm of Cu, the peak energy moves to higer energies wrt the case with only Al (from 27 keV to 39 keV).

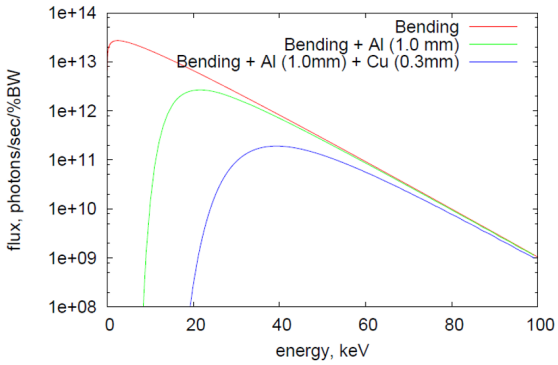

Figure 2: Spectrum of the ALBA dipole at FE34, after traversing 1 mm of Al and 0.3 mm of Cu.

Pinhole Width Measurement

One of the key systems is the pinhole itself. We use a similar design as in [5], using tungsten (W) blocks of [10x3x1] mm assembled one on top of the other, with small shims of 50, 10, and 5 µm in between (see Fig. 3). Placed vertical and horizontally, the blocks form a grid of 9 different hole sizes. Using a motorized stage, we can use one or another (pin)hole. We typically use the center hole (the one made with the shims of 10x10 µm).

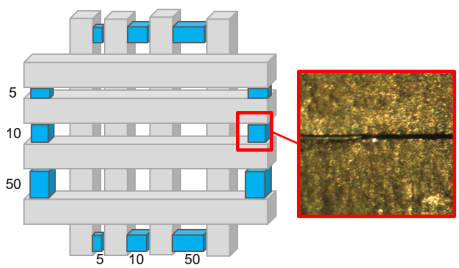

Figure 3: Left: Sketch of the pinhole block installed in FE21. Right: microscope image showing the 10 µm shim between the two W-blocks.

Prior to its installation, the different slit widths are measured with a microscope. Once installed, we repeat these measurements using the X-ray beam itself: tilting the setup from the minimum to maximum illumination, and back to minimum. The measurements results for the slits using the 10 µm spacer are summarized in Fig. 4: note that although we use 10 µm spacers, the "effective" width is actually larger (about 20 µm). This could be related to the deformation of the spacers when they are cut (see Fig. 3, right), which cannot be fully compressed using the mechanical set-up.

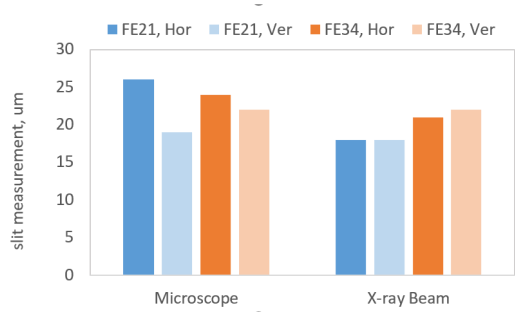

Figure 4: Measurements of the slit widths forming the pinhole in FE21 and FE34.

ANALYTICAL PSF EVALUATION

Imaging using synchrotron radiation is affected by the diffraction and blurring effects. For a given photon energy E and pinhole width w, these contributions are analytically evaluated by [5]:

$$\sigma_{\text{diff}} = \frac{\sqrt{12hc}}{4\pi}\frac{L_2}{E\cdot w}, \qquad \sigma_{\text{blur}} = \frac{w(L_1+L_2)}{\sqrt{12}L_1}, \tag{2}$$

where c is the speed of light, h is the Planck constant and L_1, L_2 are described in Fig. 1.

But the synchrotron radiation (SR) that forms the pinhole image is not monochromatic, and so Eq. (2) must take into account the spectrum given by the ALBA bending, attenuated by the Al window and Cu filter (if in use). The numerical integration of Eq. (2) is done using

$$\sigma_{\text{DIFF}} = \int \sigma_{\text{diff}}(E)P(E)dE, \qquad P(E) = \frac{N_{\text{ph}}(E)}{\int_0^\infty N_{\text{ph}}(E)\,dE}. \tag{3}$$

Here $N_{\text{ph}}(E)$ is the photon flux for a specific energy (see Fig. 2). Then, the PSF is obtained by adding these contributions in quadrature:

$$\sigma_{\text{PSF}} = \sqrt{\sigma_{\text{blur}}^2 + \sigma_{\text{DIFF}}^2 + \sigma_{\text{screen}}^2}, \tag{4}$$

where σ_{screen} is the CCD pixel size. Solving Eqs. (3) and (4), in FE21 we find σ_{PSF}=24 µm with only Al, while it goes down to 18 µm if we use 0.3 mm of Cu. For FE34 and only Al, σ_{PSF}=22 µm and it goes down to 15 µm if we use 0.3 mm of Cu. The values of FE21 are larger due to the larger magnification.

PSF CALCULATION USING SRW

For these simulations we consider the wavefront of light emitted by a point-like ("zero emittance") beam. We perform the simulations using a 10 µm horizontal and 1 µm vertical, which is a factor ~25 smaller than the real vertical size and it is a good compromise between an optimum simulation result

ISBN: 978-3-95450-241-7 ISSN: 2673-5350 doi:10.18429/JACoW-IBIC2022-WEP16

and the CPU time. The σ_{PSF} is computed in the vertical plane because this is where the smallest beam size is achieved.

Although we have seen that recently SRW allows to perform polychromatic simulations through OASYS [6], this was not the case when we first start this study. Therefore, we have done monochromatic simulations [7] at different energies (in our case, 5 different energies). These energies are chosen considering the spectrum flux in FE21 and FE34, with and w.o. Cu filter (0.3 mm). As an example, Fig. 5 shows the normalized spectrum for the FE34 case with 0.3 mm of Cu, and with the "representative" energies (red boxes).

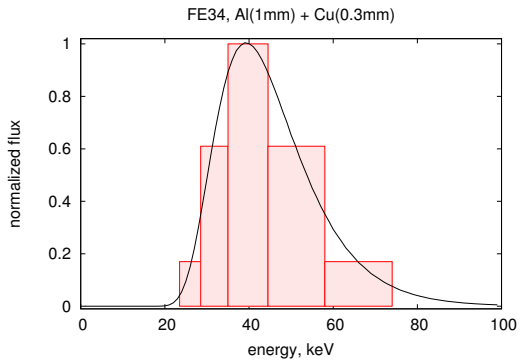

Figure 5: Normalized transmission spectra for FE34, assuming Al (1 mm) and 0.3 mm of Cu. The red squares denote the energies considered for the PSF calculation in Fig. 6.

For each these energies, SRW provides an intensity profile (Fig. 6, top), which is weighted with the values of the normalized spectrum. Next, we add these contributions in one single profile (red dots in Fig. 6, bottom). The σ_{PSF} is obtained after fitting this profile to a Gaussian function (blue line in Fig. 6 - bottom). We are currently performing polychromatic simulations using the up-to-date version of SRW to crosscheck these results.

Consistently with the analytical calculations, we obtain values of 23 and 19 µm for FE21 with and w.o. Cu, while in FE34 these are 18 and 15 µm with and w.o. Cu. Moreover, we perform this analysis for several Cu filter cases to fully characterize the PSF. Then, we fit the PSF as a function of the Cu filter thickness as shown in Fig. 7 for the case of FE21 and 5 µm slit. Then, this fit is included in the GUI that provides the beamsize in real-time in the Control Room during normal operation, so that in case operators move the Cu thickness, or change the pinhole width, the PSF is automatically updated. More details can be found in Ref. [9].

EXPERIMENTAL PSF CALCULATION

The pinhole PSF can be experimentally calculated using the Touschek lifetime, τ_T as already performed in [8]. For the ultra-relativistic case, and in ALBA conditions, we have

$$\frac{1}{\tau_T} \approx \left\langle \frac{c r_p^2 N_p}{2\sqrt{\pi}\gamma^2 \sigma_z \sigma_x \sigma_y (\Delta_E/E_0)^2} \right\rangle, \qquad (5)$$

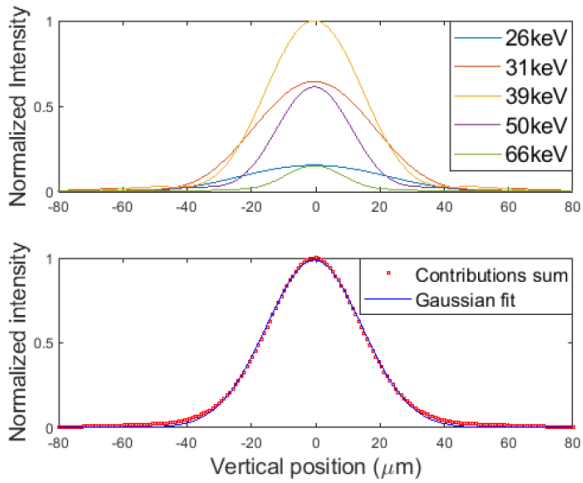

Figure 6: Top: FE34 PSF obtained at the screen for five different energies with 0.3 mm of Cu. Bottom: Sum of all PSF contributions (red dots) and Gaussian fit (blue).

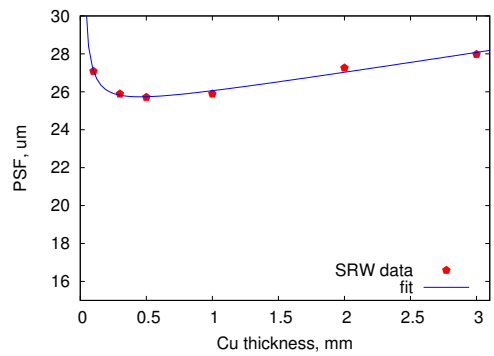

Figure 7: PSF calculation at FE21 for different Cu thickness using SRW simulations (red points) and fit (blue).

where c is the speed of light, r_p is the classical particle radius, N_{p} is the number of electrons in the bunch, σ_{z} is the bunch length, (Δ_E/E_0) is the relative energy spread. The brackets mean the average over the whole storage ring circumference. Note that Touschek lifetime is directly proportional to the average horizontal $\langle \sigma_{\mathrm{x}} \rangle$ and vertical beam sizes, $\langle \sigma_{\mathrm{y}} \rangle$.

When ALBA operates in a Touscheck dominated regime, then we can assume the measured lifetime τ is mainly the Touscheck lifetime τ_T, and so

$$\langle \sigma_{\mathrm{y}} \rangle = k \cdot \tau, \qquad (6)$$

where k is a scaling factor. If we further assume that the average vertical beam size $\langle \sigma_y \rangle$ is proportional to the beam size measured at the ALBA pinholes σ_{YAG}, then

$$\left(\frac{\sigma_{\mathrm{YAG}}}{X}\right)^2 = (k\tau)^2 + \left(\frac{\sigma_{\mathrm{PSF}}}{X}\right)^2. \qquad (7)$$

Figure 8 shows an example of such a measurement, in which the coupling is changed using different set of the skew quarupoles. At each skews settings, we measure the lifetime and the vertical beam size in both pinholes, with and w.o.

ISBN: 978-3-95450-241-7 ISSN: 2673-5350 doi:10.18429/JACoW-IBIC2022-WEP16

0.3 mm of Cu. The PSF for each case is found from the independent term in the linear fit (solid lines in Fig. 8). The final result shown in Fig. 8 is the average of 5 experiments, where the error bar includes both the fitting error as well as the spread of the measurements.

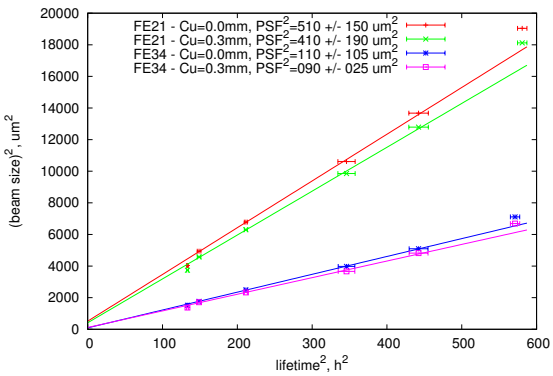

Figure 8: Lifetime evolution and beam size calculation using both pinholes for the "only Al case", and the case with "Al and Cu".

Note the large error bars in the linear fits. These stem from several reasons. First, the lifetime measurement at ALBA oscillates significantly due to the DCCT noise (see error bars in Fig. 8). Furthermore, although the measurements are performed in a regime in which the Touscheck lifetime dominates, the gas lifetime still has a non-negligible influence and so Eq. (5) is not valid in all the parameter space (this is especially relevant at high beam sizes). Finally, we note that the coupling correction is only performed with 32 skews, and this means the coupling correction is discrete and might not be uniform through the ring. This is especially relevant for low beam sizes. We note that in Fig. 8 the last and first points are not considered for the fits.

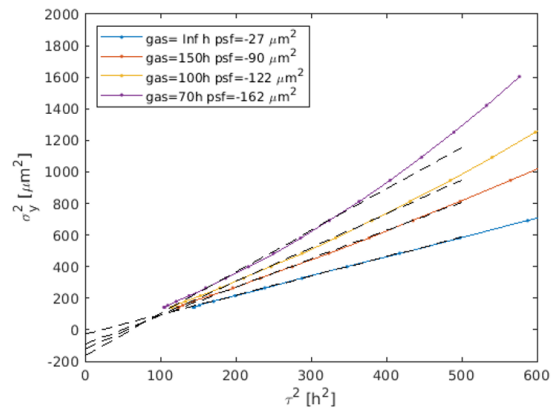

Figure 9: Lifetime evolution and expected beam size at FE34 according to the MML simulation.

Figure 9 shows a MML simulation for the FE34 case, correcting the coupling with the skew magnets and assuming different gas lifetimes. We note that even in all cases (even if we consider the gas lifetime as infinite), the expected PSF has a negative value.

RESULTS AND CONCLUSIONS

Table 2 lists the results of the PSF calculation with the three different methods for both pinholes, in case of only Al or with Al and 0.3 mm of Cu.

Table 2: Summary of the PSF Calculation at Both Pinholes Using the Three Different Methods in This Report

	FE21 Al	FE21 Al + Cu	FE34 Al	FE34 Al + Cu
Analytic	24.4	18.9	21.7	15.2
SRW	23.1	18.8	17.8	14.8
Exper.	20 ±16	20 ±15	13 ±15	13 ± 17

The values of σ_{PSF} obtained for the pinhole in FE21 are larger than the ones of pinhole in FE34 because the magnification of pinhole FE21 is larger. Despite this fact, the resolution (in terms of minimum measurable beam size) of FE21 pinhole is better than FE34. Considering that σ_{PSF}/X is the minimum beam size measurable by the pinhole camera, we obtain a minimum beamsizes of 6.5 µm for FE34, and 5.0 µm for FE21 (in the case with Cu filter of 0.3 mm).

The results using the different methods agree among them, especially between the analytical and the SRW simulations. The experimental measurements show a big error bar due to the inherent uncertainties in the experiment. We are currently performing more SRW simulations including polychromatic effects to crosscheck the results shown here.

The effect of the PSF is included in the Control Room GUI that provides in real-time the beam sizes of FE21 and FE34. The PSF is automatically updated for different hole sizes and values of the Cu thickness, as shown in [9]. Nevertheless, note that the effect of adding in quadrature σ_{PSF} to the vertical beam size is in the order of few %. Using 0.3 mm of Cu, excluding the PSF would correspond to 2.5% error in FE21, and 5% in FE34 for the typical operation values of $\sigma_y = 25$ µm. The effect of σ_{PSF} on the horizontal beam size of the image, is even smaller because $\sigma_x \sim 60$ µm.

ACKNOWLEDGEMENTS

The authors would like to acknowledge D. Heinis for the support using SRW.

REFERENCES

[1] U. Iriso, M. Alvarez, F. F. B. Fernandez, A. Olmos, and F. Perez, "Diagnostics during the ALBA Storage Ring Commissioning", in *Proc. DIPACâ€™11*, Hamburg, Germany, May 2011, pp. 280–282. https://jacow.org/DIPAC2011/papers/TUOA02.pdf

[2] L. Torino and U. Iriso, "Transverse beam profile reconstruction using synchrotron radiation interferometry", *Phys. Rev. Accel. Beams*, vol. 19, p. 122801, 2016. doi:10.1103/PhysRevAccelBeams.19.122801

ISBN: 978-3-95450-241-7 ISSN: 2673-5350 doi:10.18429/JACoW-IBIC2022-WEP16

[3] M. Siano, *et al.*, "Two-dimensional electron beam size measurements with X-ray heterodyne near field speckles", *Phys. Rev. Accel. Beams*, vol. 25, p. 052801, 2022. doi:10.1103/PhysRevAccelBeams.25.052801

[4] SRW, https://www.esrf.fr/Accelerators/Groups/InsertionDevices/Software/SRW

[5] P. Elleaume, C. Fortgang, C. Penel, and E. Tarazona, "Measuring Beam Sizes and Ultra-Small Electron Emittances Using an X-ray Pinhole Camera", *J. Synchrotron Radiat.*, vol. 2, pp. 209–214, 1995. doi:10.1107/S0909049595008685

[6] OASYS, https://www.aps.anl.gov/Science/Scientific-Software/OASYS

[7] I. Mases, A. Garcia-Santiago, and U. Iriso, "Characterization of the Point Spread Function for the X-ray pinhole cameras at ALBA Synchrotron", Treball Final de Grau, Univ. Autònoma Bellaterra, 2020. http://hdl.handle.net/2445/176714

[8] L. M. Bobb, A. F. D. Morgan, and G. Rehm, "Performance Evaluation of Molybdenum Blades in an X-ray Pinhole Camera", in *Proc. IBICâ€™16*, Barcelona, Spain, Sep. 2016, pp. 795–798. doi:10.18429/JACoW-IBIC2016-WEPG63

[9] A. A. Nosych and U. Iriso, "Real-Time Beam Detection and Tracking From Pinhole Imaging System Based on Machine Learning", in *Proc. IBICâ€™21*, Pohang, Korea, Sep. 2021, pp. 272–275. doi:10.18429/JACoW-IBIC2021-TUPP28